IEEE Photonics Journal
An IEEE Photonics Society Publication

Statistical Dynamics of Coherent Quantum Systems Operating in the Presence of Quantum Noise

Volume 9, Number 1, February 2017

William C. Lindsey, ***Life Fellow, IEEE***

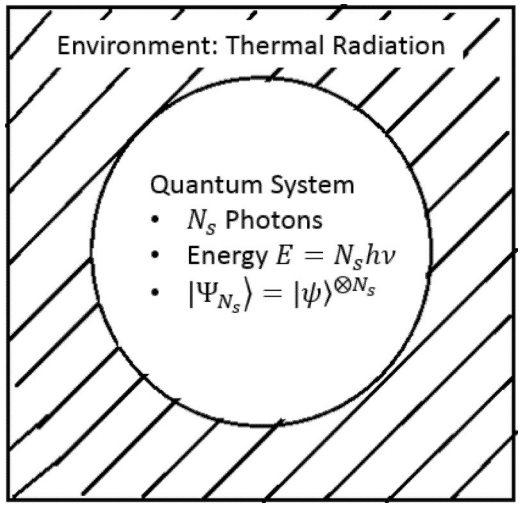

DOI: 10.1109/JPHOT.2017.2649220
1943-0655 © 2017 IEEE

IEEE photonics SOCIETY

IEEE

Statistical Dynamics of Coherent Quantum Systems Operating in the Presence of Quantum Noise

William C. Lindsey, ***Life Fellow, IEEE***

Department of Electrical Engineering, University of Southern California, Los Angeles, CA 90089-2565 USA

DOI:10.1109/JPHOT.2017.2649220

Manuscript received August 23, 2016; accepted December 23, 2016. Date of publication January 9, 2017; date of current version January 26, 2017. This work was supported by the Department of Electrical Engineering Systems, University of Southern California, Los Angeles, CA 90089-2565, USA. Corresponding author: W. C. Lindsey (e-mail: wclindsey@gmail.com).

Abstract: A statistical characterization of the quantum state of polarization for a coherent quantum system disturbed by quantum noise is presented. The composite quantum system consists of an integer number N_s of mutually polarized photons disturbed by quantum noise which consists of an average number $\mathcal{N}$ of thermal radiation quanta plus the zero-point energy fluctuations. The interacting and coupled dynamics of the quantum system polarization is modeled by mutually coupled energy balanced stochastic differential equations mimicking the motion of Huygens mutually coupled pendulum clocks. The Markovian nature of the quantum noise allows one to use the Fokker–Planck (FP) apparatus to develop a coherency distribution which lives on a Clifford horn torus. Using this distribution, distributions for the Quantum State-of-Polarization, the Quantum Degree-of-Polarization, the circular moments, and the azimuthal and longitudinal polarization state jitters are derived. It is shown that the stable polarization states of quantum system equilibrium define a Bravais lattice in phase space. From this perspective, it is shown that quantum polarization interruptions are at the heart of certain quantum decoherence effects, e.g., polarization slips and flips, while pendula-like clock synchronization is at the heart of maintaining and sustaining coherency among the parts (photons) of coherent quantum systems. A classical world to quantum world "transition boundary" is identified as a function of quantum system parameters. This function is used to partition the electromagnetic spectrum into three disjoint regions of operation: a classical, a transition, and a quantum communications region. The results presented will find applications to the problem of evaluating single and multiphoton quantum communication system performance and in the system engineering design of quantum communication systems and a quantum internet connecting quantum computers.

Index Terms: Quantum polarization, coherence, quantum synchronization, polarization qubit flips, phase flips and slips, frequency decoherence, symmetric sector, Bravais Lattice, Fokker-Planck (FP), Majorana.

1. Introduction

Polarization of light in classical and quantum optics is of fundamental significance in several quantum technology fields [1], [2]. The Degree-of-Polarization (DoP) is often used as a key system performance measure for classical as well as in quantum communications [3], [4]. The term depolarization implies a decrease in the DoP of a light beam traversing an optical signal path and

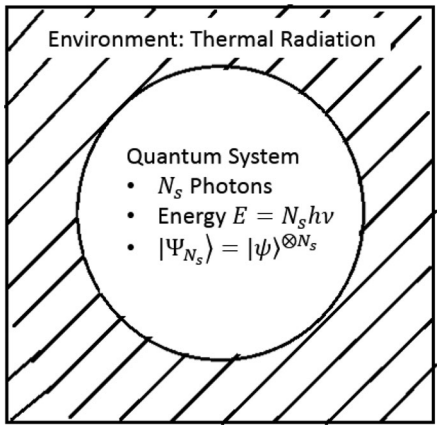

Fig. 1. Composite quantum system concept.

leads to a loss in beam coherence that is often referred to as decoherence [5], [6]. In [7] and [8], decoherence was addressed by coupling the field modes to a randomly distributed atomic bath and a linear master equation was derived and investigated for a single mode [7]. In [8], Kilmov *et al.*, introduced a phased-space perspective; the linear master equation was solved for operation in the high temperature quasi-classical region for the Glauber-Sudarshan P-function [9]. From a system engineering perspective, this P-function is difficult to investigate numerically and is not compatible for use in assessing quantum communication system performance [10]. Moreover, the celebrated Sudarshan-Glauber P phase-space representation fails to be a legitimate probability density function [10], [11].

In this paper, coherence probability distributions which define the Quantum State of Polarization (Q-SoP) and the Quantum Degree of Polarization (Q-DoP) are derived for coherent Quantum Systems operating in the presence of quantum noise [12]. The Q-SoP and Q-DoP are modeled from a phase-space perspective using coupled nonlinear stochastic differential equations mimicking coupled Huygens pendulum clocks [13], [14]. The N_s-qubit quantum polarization states are modeled by their Majorana representations [15]–[17] taken from the symmetric sector of N_s-qubits [18]–[22]. These states are also referred to as SU(2) coherent spin states [16]. Herein, the set of states chosen from this sector are called "coherent polarized states" because of their closeness to coherent communication signals employed in the implementation of classical coherent communication systems.

The Quantum System (QS) considered in the this paper is composed of N_s mutually polarized photons. Quantum states which characterize this system are dubbed "coherent polarized states." This system is assumed to live in a quantum noise environment consisting of thermal radiation composed of an average number $\mathcal{N}$ of thermal quanta; see Fig. 1. As such, the QS interacts with this environment. This interaction causes degradations in QS coherence, creates quantum polarization disturbances, e.g., polarization qubit flips and slips, and causes qubit transmission errors in quantum communication systems [23]–[26]. In addition, there exist degradations to the Q-SoP and Q-DoP due to phase jitters associated with the azimuthal and longitudinal phase components [5], [6]. Such degradations can destroy the relative phase between the components of a linear superposition state and so does frequency decoherence due to frequency instabilities [6].

Quantum communications depends exquisitely on QS parts remaining coherent for time intervals longer than the time duration of a qubit. Interaction between a pristine qubit and its environment threatens destruction of qubit coherency. Polarized photons (polarization qubits) are perhaps the best quantum information carrier to use in the implementation of quantum communication systems and a quantum internet connecting quantum computers [10], [25]–[28].

The problem of quantifying system performance metrics for use in quantum system engineering design in the presence of quantum noise is of great practical importance. Analogous with

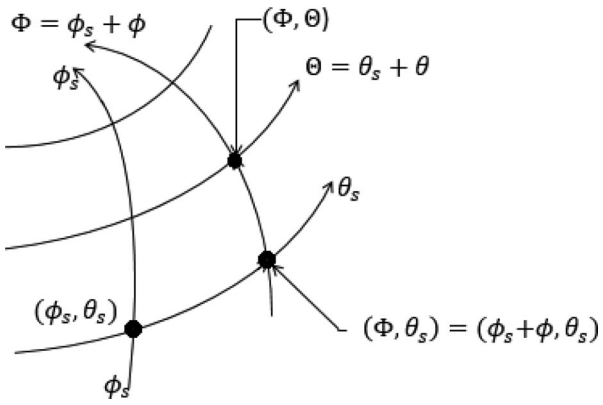

Fig. 2. Polarized signal state (ϕ_s, θ_s) and disturbed polarization state (Φ, Θ).

classical communication system performance, quantum communication system performance may not be achievable due to the presence of quantum noise if there is not sufficient state energy. Therefore, some form of scalable "quantum signal energy" design requirement will have to be met. In this paper, coherent polarization states are suggested which accommodate the requirements of signal energy scalability. Such coherent polarization states are analogous with coherent signals used in classical communications and are not to be confused with Glauber's coherent states [9].

More quantitatively speaking, let $\phi(t) = \Phi(t) - \phi_s$ and $\theta(t) = \Theta(t) - \theta_s$ characterize the random deviations in the Q-SoP $(\Phi(t),\ \Theta(t))$ from the pristine polarization configuration (ϕ_s, θ_s). In particular, let the joint random processes $(\Phi(t),\ \Theta(t))$ characterize the instantaneous value of the Q-SoP of the QS, see Fig. 2. Due to thermal radiation, this polarization state (Φ, Θ) undergoes diffusion with the passage of time leading to degrading decoherence effects. The joint probability distribution of these two joint processes will be refered to as the conditional joint probability distribution $P(\Phi, \Theta|\phi_s, \theta_s)$ of the Q-SoP and $P(\phi, \theta)$ as the QS coherency distribution. From the coherency distribution, the Q-DoP distribution is derived.

In this paper, the dynamical behavior of these joint random processes are modeled by stochastic differential equations which mimic the dynamics of mutually-coupled "massless" pendulums whose quantum energetic forces, or interacting forces, remain balanced. When considered jointly, they characterize random phase trajectories which establish the various QS performance distributions. When the correlation time of the quantum noise processes is shorter than the duration of a qubit, say T_{qb}, the processes can be approximated as jointly Markovian. In this regard, the Fokker-Planck (FP) apparatus can be used to obtain a statistical characterization of the system performance metrics, in particular, the coherency and Q-SoP and Q-DoP distributions. The coherence distribution is shown to live on a Clifford horn torus phase-space. Phase plane analysis exhibits periodic attraction and repulsion points of polarization stability. The attractor points are stable polarization states and the repulsion points characterize unstable polarization states. In the absence of noise, the stable points define a Bravais lattice. With the passage of time, the noise causes the polarization state of the quantum system to flip to an antipodal state or to make full encirclements (clockwise and counterclockwise) called polarization slips at random points in time. The coherency distribution is plotted in three dimensions for various values of the composite system parameters. In addition, the Q-SoP distribution is derived and the distribution of the z-component P_z of polarization is presented along with the polarization jitters.

This paper is written from a quantum communications perspective in that the parameter space for the composite quantum system model is identified in terms of those parameters familiar to both classical and quantum communication system engineers [10], [25], [26], [29]. The paper is organized as follows. Section II presents the QS model considered herein. Section III develops the dynamical models for the composite quantum system in terms of stochastic differential equations.

Phase plane stability analysis in the absence of noise is presented and the quantum phase noise model developed. Section IV establishes the FP equation from which the coherency and the Q-SoP distributions are derived. Section VI develops the Q-DoP distribution and other related composite QS marginal and conditional distributions. Section VII also presents the polarization jitter analyses, circular moments, and frequency decoherence averages. Concluding remarks are given in Section VIII.

2. Quantum System Model

In this section, the quantum states which characterize the QS under consideration herein are defined assuming the QS is composed of N_s polarized photons. These states will be referred to as "coherent polarized states" for reasons which will become obvious and are not to be confused with Glauber's coherent states [9].

Let $(\phi_{sk},\ \theta_{sk})$ define the polarization orientation of the k^{th} photon, $k = 1,\ 2,\ \ldots., N_s$ and let the set $S_k(\phi_{sk},\ \theta_{sk}) = \{(\phi_{sk},\ \theta_{sk}) : 0 \leq \phi_{sk} \leq 2\pi, 0 \leq \theta_{sk} \leq \pi\}$ define the corresponding polarization phase-space. In this space, one can represent a "polarization qubit" as a two-level system in SU(2) as follows:

$$|\psi_k\,(\phi_{sk},\ \theta_{sk})\ = \cos\,(\theta_{sk}/2)|\,0 + e^{i\phi_{sk}} \sin\,(\theta_{sk}/2)\,|1. \tag{1}$$

Geometrically speaking, the point $(\phi_{sk},\ \theta_{sk})$ can be used to define unit vectors in SO(3) as points on the Bloch sphere. Further, assume that the configuration states $|\psi_k(\phi_{sk},\ \theta_{sk})$ are separable, [30], [31]. Then a scalable state in the quantum system can be written as the Kronecker product

$$|\Psi_{Ns}\,(\boldsymbol{\phi_s},\ \boldsymbol{\theta_s}) = |\psi_1\,(\phi_{s1},\ \theta_{s1})\otimes|\,\psi_2\,(\phi_{s2},\ \theta_{s2})\otimes\ldots\otimes|\psi_{N_s}\,(\phi_{sN_s},\ \theta_{sN_s}) \tag{2}$$

where $\boldsymbol{\phi_s} = (\phi_{s1}, \phi_{s2}, \ldots \phi_{sN_s})$ and $\boldsymbol{\theta_s} = (\theta_{s1}, \theta_{s2}, \ldots, \theta_{sN_s})$ are called polarization coherency vectors. If all signal photons are prepared in synchronicity such that $\phi_s = \phi_{sk}$ and $\theta_s = \theta_{sk}$ for all k, the above state can be written as

$$|\boldsymbol{\Psi}_{Ns}\,(\boldsymbol{\phi_s},\ \boldsymbol{\theta_s}) = |\psi(\phi_s,\ \theta_s)^{\otimes N_s} \tag{3a}$$

where $\boldsymbol{\phi_s} = (\phi_s, \phi_s, \ldots, \phi_s)$ and $\boldsymbol{\theta_s} = (\theta_s, \theta_s, \ldots, \theta_s)$. Thus, a "coherent polarized state" $|\Psi_{N_s}(\boldsymbol{\phi_s},\ \boldsymbol{\theta_s})$ is specified by the polarization state (ϕ_s, θ_s), its frequency ν, the number of photons N_s and its energy $E = N_s h\nu$. The representation in equations (2) and (3) belongs to the symmetric sector of N_s -qubits. It is known that quantum states in this sector are characterized by two key parameters, viz., the diversity degree and the degeneracy configuration [18]. This sector has been investigated in several recent studies [16]–[21]. For the separable SU(2) coherent states in (3), the Majorana constellation [15], [16] collapses to a single point on a unit sphere such that the spin spherical representation generalizes the one-half Bloch sphere [16]. In this regard, it is noted that (2) and (3) characterize a particular symmetric sector of N_s-qubits with degeneracy configuration N_s and diversity d = 1 [32]. The quantum states in (3) are attractive for quantum communications applications because their energy in the state scales with N_s, [10], [25], [26], [32]. Placement of this QS in its environment forms the Composite Quantum System under consideration, see Fig. 1. In the presence of quantum noise, the pristine coherent polarized state in (3*a*) transforms, at time t, to the "noisy" state

$$|\boldsymbol{\Psi}_{\mathbf{N_s}}\,(\boldsymbol{\Phi}, \boldsymbol{\Theta}) = |\psi\,(\Phi, \Theta)^{\otimes N_s} \tag{3b}$$

for all the $t \geq t_0$. Here the environment is assumed to be that of thermal radiation and will be characterized as quantum noise. Moreover, "coherent polarized states" $|\Psi_{N_s}(\boldsymbol{\phi_s}, \boldsymbol{\theta_s})$ are analogous with or counterpart to coherent signals used in classical communications. Engineering realization of "coherent polarized states" in (3) have been advanced in a nonlinear process dubbed "coherent photon conversion" and is based upon interacting bosonic fields [33]–[35].

3. Dynamical Model of Coherent Quantum Systems Operating in Quantum Noise

The dynamical equations which characterize the statistical behavior of coherent quantum systems operating in the presence of quantum noise are derived in this section. Let $\phi(t) = \Phi(t) - \phi_s$ characterize the longitudinal (toroidal) phase deviation trajectories and $\theta(t) = \Theta(t) - \theta_s$ characterize the azimuthal (poloidal) phase deviation trajectories due to the background quantum noise (thermal radiation). The disturbed polarization trajectories $\Phi(t)$ and $\Theta(t)$ are random processes, see Fig. 2. Taken as pairs $(\phi(t),\ \theta(t))$ and $(\Phi(t), \Theta(t))$ these representative points undergo diffusion as they move randomly over the phase-space $(|\phi(t)| \leq \infty, |\theta(t)| \leq \infty)$ and $(|\Phi(t) = \phi_s + \phi(t)| \leq \infty,\ |\Theta(t) = \theta_s + \phi(t)| \leq \infty)$. In fact, the random deviation process serve to characterize the coherency distribution while the polarization components $(\Phi(t),\ \Theta(t))$ serve to characterize the Q-SoP.

Now consider the dynamical aspects of these motions. Assume that this motion mimics that of "massless" pendulums driven away from the pristine polarization state $(\phi_s,\ \theta_s)$ by zero mean quantum noise processes, $N_\Phi(t)$ and $N_\theta(t)$. Assume further that there exists resisting "quantum energetic forces" acting on the coherent polarized state (photon packet) so as to maintain its prepared polarization state $(\phi_s,\ \theta_s)$. There are two such forces. First, there are the mutually-coupled energetic restoring forces which maintains the photons azimuthal and longitudinal positions, namely, the energetic forces $E\cos(\Theta - \theta_s)\sin(\Phi - \phi_s) = N_s\hbar\omega_c cos\theta sin\phi$ and $E\cos(\Phi - \phi_s)\sin\cos(\Theta - \theta_s) = N_s\hbar\omega_c cos\phi sin\theta$. Second, there exists viscous frictional energetic forces $(\hbar\dot{\Phi},\ \hbar\dot{\Theta})$ and $(\hbar\dot{\phi},\ \hbar\dot{\theta})$. Third, there are the frequency ω_c decohering processes $\dot{\psi}_\phi(t)$ and $\dot{\psi}_\theta(t)$ present in the photon generator. Herein, it is assumed that $\dot{\psi}_\phi = \dot{\psi}_\theta = \hbar\Delta\omega_c = 2\pi\hbar\Delta\nu_c$ where $\Delta\nu_c$ characterizes a bias offset frequency relative to center frequency $\omega_c = 2\pi\nu_c$ and acts as a frequency decohering effect on the polarization state $(\phi_s,\ \theta_s)$. If one insists that these quantum energetic forces be balanced against those of quantum noises, one can write the dynamical equations of energy exchange for the polarization state representative points $[\Phi(t), \Theta(t)]$ at time t as

$$\hbar\dot{\Phi} + E\cos(\Theta - \theta_s)\sin(\Phi - \phi_s) = \hbar\dot{\psi}_\phi(t) + \sqrt{\hbar}N_\Phi(t) \tag{4}$$

$$\hbar\dot{\Theta} + E\cos(\Phi - \phi_s)\sin(\Theta - \theta_s) = \hbar\dot{\psi}_\theta(t) + \sqrt{\hbar}N_\Theta(t).$$

Upon dividing by $\hbar$ one gets the equivalent phase-space equations

$$\dot{\Phi} + \omega_c N_s\cos(\Theta - \theta_s)\sin(\Phi - \phi_s) = \Delta\omega_c + N_\Phi(t)/\sqrt{\hbar} \tag{5}$$

$$\dot{\Theta} + \omega_c N_s\cos(\Phi - \phi_s)\sin(\Theta - \theta_s) = \Delta\omega_c + N_\Theta(t)/\sqrt{\hbar}.$$

Since $\dot{\phi} = \dot{\Phi}$ and $\dot{\theta} = \dot{\Theta}$, (5) can be written in terms of the "decoherency process" $[\phi(t), \theta(t)]$ and the depolarizing quantum phase noise processes, viz.,

$$\dot{\phi} - \Delta\omega_c + \omega_c N_s cos\theta sin\phi = n_\Phi(t) \tag{6}$$

$$\dot{\theta} - \Delta\omega_c + \omega_c N_s cos\phi sin\theta = n_\Theta(t)$$

where $n_\Phi(t) = N_\Phi(t)/\sqrt{\hbar}$ and $n_\Theta(t) = N_\Theta(t)/\sqrt{\hbar}$ relates the quantum phase noise processes to the thermal background radiation processes.

3.1. Polarization State Stability Analysis

Dynamics of the Q-SoP for the QS can be understood using phase plane techniques and the stability theorem of nonlinear mechanics [36]. Without loss in generality, assume that $\Delta\omega_c = 0$ and that $N_\Phi(t) = N_\Theta(t) = 0$ in (5). Thus, (5) reduces to

$$\dot{\phi}/\omega_c N_s = \dot{\Phi}/\omega_c N_s = -\cos(\Theta - \theta_s)\sin(\Phi - \phi_s) \tag{7}$$

$$\dot{\theta}/\omega_c N_s = \dot{\Theta}/\omega_c N_s = -\cos(\Phi - \phi_s)\sin(\Theta - \theta_s).$$

The simultaneous solution of (7) for ϕ and θ leads to two identical second-order differential equations of the form $\ddot{x} - \cot(x/2)\dot{x}^2 + \omega_c^2 N_s^2 sinx = 0$ where $x = 2\phi$ or 2θ. This is the pendulum equation with damping proportional to the negative of the square of the angular velocity. Also note that the sum θ_+ and difference θ_- ($\theta_\pm = \phi \pm \theta$) obey "massless" pendulum equations. Q-SoP equilibrium conditions occur at Q-SoP (Φ, Θ) where the conditions $\dot{\phi} = \dot{\Phi} = \dot{\theta} = \dot{\Theta} = 0$ or equivalently where $\dot{\phi}/\dot{\theta} = \dot{\Phi}/\dot{\Theta} = 0/0$ are met. Such points represent polarization state singularities and are subject to analysis. Now the conditions $\dot{\Phi}/\dot{\Theta} = \dot{\phi}/\dot{\theta} = 0/0$ will occur when $\sin(\Phi - \phi_s) = \sin(\Theta - \theta_s) = 0$ or when $\cos(\Phi - \phi_s) = \cos(\Theta - \theta_s) = 0$. Now $\sin(\Phi - \phi_s) = \sin(\Theta - \theta_s) = 0$ at ($\Phi_n - \phi_s = 2n\pi$, $\Theta_k - \theta_s = 2k\pi$) or at odd multiples of π from these points, say ($\Phi_n - \phi_s = (2n + 1)\pi$, $\Theta_k - \theta_s = (2k + 1)\pi$) for n and $k = 0, \pm1, \pm2, \ldots$ These points (Φ_n, Θ_k) constitute stable polarization states because the characteristic equation, obtained using the ratio $\dot{\theta}/\dot{\phi} = d\theta/d\phi = \tan\theta \cot\phi$, has negative characteristic real roots [36]. This set of points are denoted respectively by symbols " • and ◦." Furthermore, unstable polarization saddle points "SP" occur at the points ($\Phi'_n - \phi_s = (n + 1/2)\pi$, $\Theta'_k - \theta_s = (k + 1/2)\pi$) where $\cos(\Phi'_n - \phi_s) = \cos(\Theta'_k - \theta_s) = 0$ because the roots of the characteristic equation are positive and negative. Other unstable polarization states occur at singular points ($\Phi'_n - \phi_s = 2n\pi$, $\Theta'_k - \theta_s = (2k + 1)\pi$) where $\cos(\Phi'_n - \phi_s)\sin(\Theta'_k - \theta_s) = 0$ or at points ($\Phi'_n - \phi_s = (2n + 1)\pi, \Theta'_k - \theta_s = 2k\pi$) where $\sin(\Phi' - \phi_s)\cos(\Theta' - \theta_s) = 0$. These points are unstable qubit phase flips because the roots of the characteristic equations are both positive and are denoted by the symbol "•," Using (7), the phase-space trajectories ($\Phi(t)$, Θ(t)) with time as a parameter are readily determined from the ratio $d\phi/d\theta = d\Phi/d\Theta = tan\phi/tan\theta$ by integration. The variables are separable; integrating from ($\phi_o = \Phi_o - \phi_s$, $\theta_o = \Theta_o - \theta_s$) at time t_o, the polarization state solution curves [($\phi(t) = \Phi(t) - \phi_s$, $\theta(t) = \Theta(t) - \theta_s$] at time t are given by the phase-space equation as follows:

$$|\sin(\phi(t))/\sin(\theta(t))| = |\sin(\phi_o)/\sin(\theta_o)|.$$

Mod 2π solution curves found from the phase-space equation above are shown in Fig. 3 for various initial conditions. Each solution curve corresponds to an initial condition and the arrows indicate the direction of increasing time starting with $t = t_o$. From Fig. 3(a), observe that the separatrix solution curves containing the saddle points separate the phase-space into regions where all other solution curves tend to singularities located at the origin or to the four corners of the square flat torus, i.e., from (ϕ_o, θ_o) at $t = t_o$, the solution curves move into one of the stable singularities as t increases. One of these stable points may be considered as "right-hand" circular polarization and the other as "left-handed." The antipodal nature of these stable points are easily visualized when the flat torus in Fig. 3(a) is folded into the Clifford horn torus. Furthermore, the Mod 2π solution curves in Fig. 3(a) replicate themselves throughout the ϕ-θ phase-space and the trajectories in Fig. 3(a) are symmetric about the $\theta = 0$ axis. As such, they can be folded Mod 2π in ϕ and Mod π in θ. When this is done, the phase-space trajectories in Fig. 3(a) become those shown in Fig. 3(b) where the direction of phase-space motion follows again the arrows. This phase-space motion in Fig. 3(b) can further be folded onto the spheres shown in Fig. 3(c) and (d) where one observes the direction of flow on the sphere. When quantum noise is present, the arrows point in the direction of "probability flow" which will be quantified in Section IV.

The set of stable points can be regarded as "attractor points" while the set of unstable points can be regarded as "repulsion points." When plotted in the Euclidean phase-space, the stable polarization states form the central-square Bravais lattice illustrated in Fig. 4 below. Moreover, the stable polarization states specified by even multiples are antipodal with respect to those at odd multiples of π, i.e., the odd multiples of π represents "polarization flips" relative to the prepared polarization state (ϕ_s, θ_s). The stable states that are even multiples of π away from (ϕ_s, θ_s) are stable but represent "polarization slips." Stated another way, the attractor points occurring at even multiples of π represent "in-phase" attractor points of pendula synchronization while the stable points occurring at odd multiples of π represent "out-of-phase" attractor points of pendula synchronization. Interpreted, with respect to Huygens pendulum clock experiment, the "out-of-phase" synchronization points are analogous with Huygens observation that his two clocks would synchronize 180 degrees out of phase, i.e., one clock would say "tick" while the other would say "tock" [10], [11]. When $\Delta\omega_c \neq 0$,

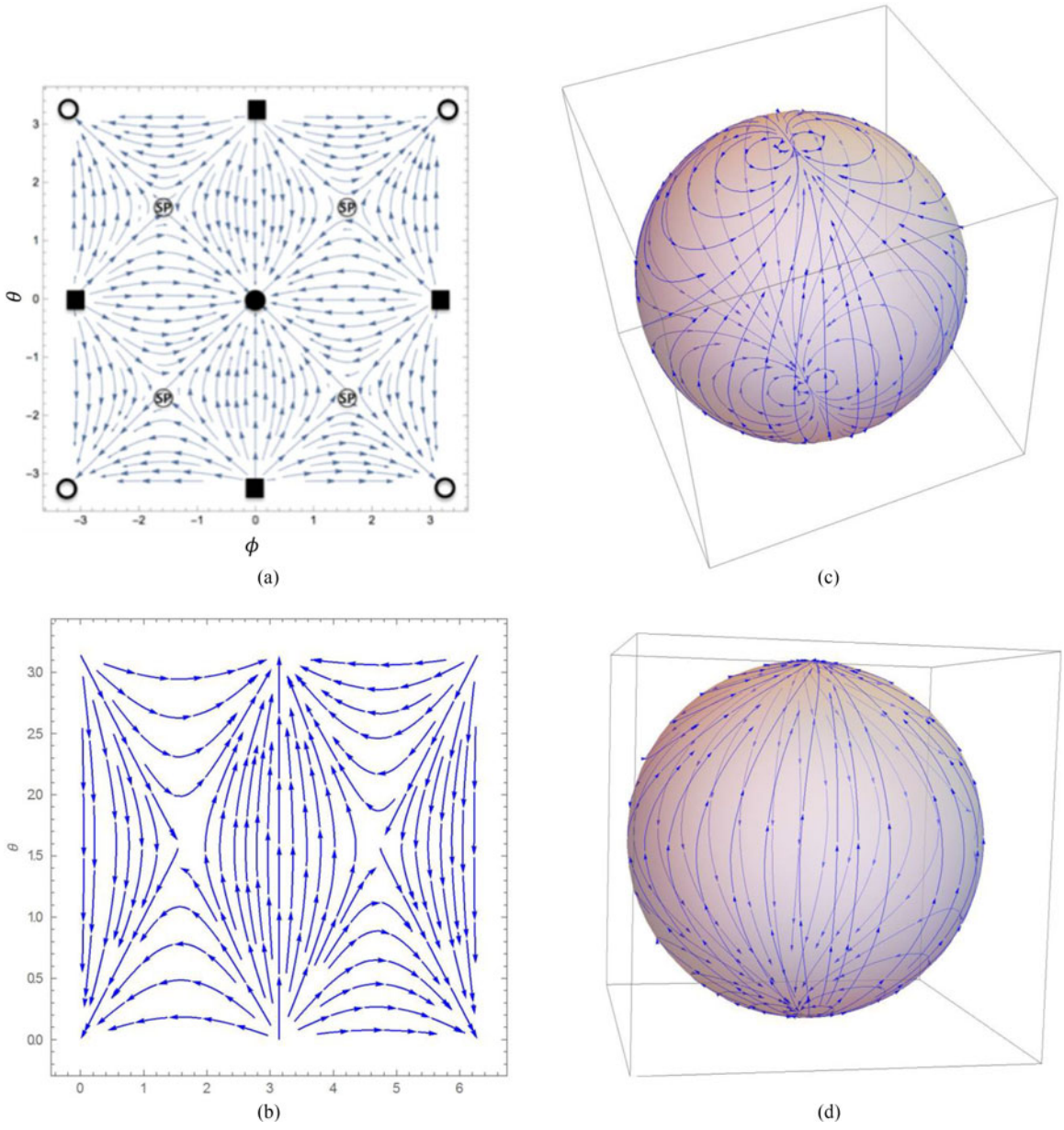

Fig. 3. Polarization state phase space trajectories relative to (ϕ_s, θ_s). (a) Mod 2π in ϕ *and* θ. (b) Mod 2π in ϕ, Mod π in θ. (c) North and South Pole views. (d) Equatorial view.

a repeat of the above analysis shows that equilibrium points occur if

$$\left|\left(\dot{\Phi} - \Delta\omega_c\right)/\omega_c N_s\right| = \left|\left(\dot{\Theta} - \Delta\omega_c\right)/\omega_c N_s\right| \leq 1.$$

If $|(\dot{\Phi} - \Delta\omega_c)/\omega_c N_s| = |(\dot{\Theta} - \Delta\omega_c)/\omega_c N_s| > 1$, no equilibrium points exist and quantum system coherency is not achievable due to frequency decoherence.

In the same way, implicit temporal solutions are found from $d\phi/sin\phi = cos\theta(t)dt$ and $d\theta/sin\theta = cos\phi(t)dt$. These integrate to

$$\tan\left(x\left(t\right)/2\right)/\tan\left(x_o/2\right) = \exp(-\Omega\int_{t_o}^{t} cos\, y\left(t\right)dt) \leq \lim_{t\to\infty} \exp\left(-\Omega\left(t - t_0\right)\right)$$

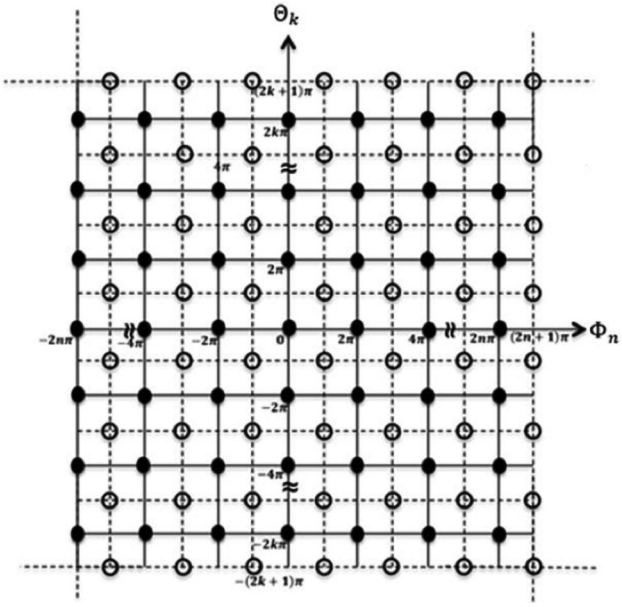

Fig. 4. Bravais lattice of stable polarization states with $\phi_s = \theta_s = 0$ (" • " even multiples of π ; " ◦ " odd multiples of π).

where $\Omega = \omega_c N_s$, $x(t) = \phi(t)$ when $y(t) = \theta(t)$ or $x(t) = \theta(t)$ when $y(t) = \phi(t)$ and $x_o = \phi_o$ when $y_o = \theta_o$ or $x_o = \theta_o$ when $y_o = \phi_o$. In limit as $t \to \infty$, then $(\phi(t), \theta(t)) \to (0, 0)$ and $(\Phi(t), \Theta(t)) \to (\phi_s, \theta_s)$. For $\Omega(t - t_o) \approx \Omega T_f = 2\pi$, these steady state values are essentially reached when $v_c T_f = 1/N_s$ which says for single photon quantum comm $v_c T_f = 1$.

3.2. Quantum Phase Noise Model

In [36], Helstrom shows that the thermal radiation process possesses the Planck spectral density function

$$S_P(\omega) = \hbar\omega \mathcal{N}(\omega) = \hbar\omega[\exp(\hbar\omega/kT^\circ - 1]^{-1}. \tag{8}$$

Here, k is Boltzmann's constant, and T° represents the temperature of the background environment, K°. From a quantum communications perspective, one identifies four key system parameters: $v_o = \omega_o/2\pi = kT^\circ/h$ is the characteristic frequency of the quantum channel, $\tau_{th} = 1/v_o$ is the thermal noise correlation time, $N_0 = kT^\circ$ is the classical white noise spectral level and $R_{qb} = E_{qb}/N_0 = hv/kT^\circ$ is the qubit energy-to-noise ratio. By adding the zero-point energy fluctuations level $Z_o = \hbar\omega/2$ to Planck's spectrum in (8), one obtains the quantum mechanical noise spectral densities

$$S_N(\omega) = \hbar\omega(\mathcal{N}(\omega) + 1/2) = (\hbar\omega/2)\coth(\omega/2\omega_o) = S_{N_\phi}(\omega) = S_{N_\theta}(\omega) \tag{9}$$

and the quantum mechanical phase-noise spectral density becomes

$$S_p(\omega) = S_N(\omega)/\hbar = (\omega/2)\coth(\omega/2\omega_o). \tag{10}$$

Therefore, the correlation function $R_N(\tau)$ of the thermal radiation is given by

$$R_N(\tau) = \hbar R_p(\tau)\ R_N(\tau) = \int_{-\infty}^{\infty} (\hbar\omega/2)\coth(\omega/2\omega_o) e^{j\omega\tau} d\omega/2\pi. \tag{11}$$

This integral cannot be placed into closed form. However, for quantum communications applications, the communications bandwidth W Hz needed around the channel center frequency v_c will support a quantum communication rate $\mathbb{R}_{qb} = 1/T_{qb} \cong W$ qubits/sec, where T_{qb} is the time

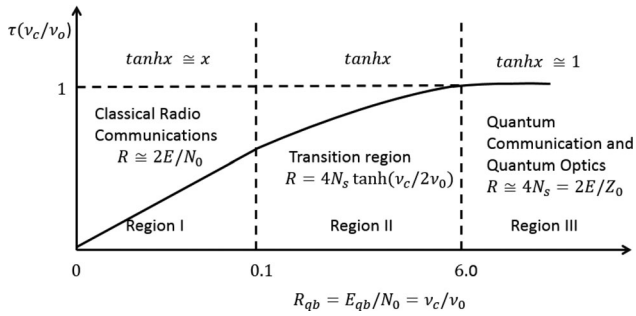

Fig. 5. Partitioning the electromagnetic spectrum as a function of the energy-per-qubit-to-noise ratio.

per qubit. Thus, the time scale τ_s of the signal motion is $\tau_s = 1/Wsec$. In the region of great interest for quantum communications, $\tau_s \ll \tau_{th}$ and the spectral function and the quantum noise spectral density $S_N(\omega)$ can be considered constant over the spectral region of interest. This says, in the region of validity, that $W\tau_{th} = W/\nu_o < 1$ or $\nu_o T_{qb} > 1$ so that (11) reduces to

$$R_N(\tau) = \left(\frac{\hbar\omega_c}{2}\right) \coth\left(\frac{\omega_c}{2\omega_o}\right) \int_{-\infty}^{\infty} \frac{\exp(i\omega\tau)\, d\omega}{2\pi} \tag{12}$$

or the quantum mechanical noise and phase noise processes are delta-correlated, i.e.,

$$R_N(\tau) = \hbar R_p(\tau) = N_{oe}\delta(\tau) \tag{13}$$

where $N_{oe} = (\hbar\omega_c/2)\coth(\omega_c/2\omega_o)$ sets the quantum white noise spectral level that is analogous with the $N_0 = kT^\circ$ level used in classical communications. In fact, in the high temperature region $\mathcal{N}(\omega_c) \cong N_0$. Furthermore, in the absence of signal photons $N_s = 0$ in (5), the trajectories $\Phi(t)$ and $\Theta(t)$ characterizes quantum Brownian motions. Using (13) another key quantum system performance parameter is identified, viz., the photon packet energy-to-quantum noise ratio

$$R = 2E/N_{oe} = 4N_s/(2\mathcal{N}+1) = 4N_s \tanh(\nu_c/2\nu_o) = 4N_s \tanh(R_{qb}/2) \tag{14}$$

where $\mathcal{N} = \mathcal{N}(\omega_c)$ is the average number of noise quanta present in the environment. Notice from (14) that $2E/N_o \le R \le 2E/Z_o = 4N_s$ for $0 \le T^\circ \le \infty$.

The function $\tau(\nu_c/\nu_o) = \tanh(\nu_c/2\nu_o)$ can be regarded as a classical-world to quantum-world "transition boundary function" [5], [6]. This function suggests a smooth and continuous transition between the two worlds as a function of the frequency operating point, see Fig. 5. In particular, for communications applications, this transition function can be used to partition the electromagnetic spectrum into three disjoint regions, viz., Region I for classical communications (or high temperature region), Region II (moderate temperature) where quantum effects begin to manifest themselves and Region III, the low temperature or high frequency quantum communications region, see Fig. 5. In the high temperature region $\nu_c/\nu_o \le 0.1$ and $R = 2E/N_0$ sets the achievable performance. In the low temperature Region III, $\nu_c/\nu_o \ge 6$ and $R = 4N_s = 2E/Z_0$ sets the irreducible noise performance due to zero-point energy fluctuations. Notice in Region III, $R \approx 4N_s$. Hence, for single-photon communications, $R = 4$ sets the zero-point irreducible quantum noise performance limit.

4. Characterization of the Fokker-Planck Equation and Its Solution

As shown in the previous section, over the time scales and spectral bandwidths of interest the noise processes $N_\Phi(t)$ and $N_\Theta(t)$ can be approximated as zero mean, independent, white quantum noise processes. Hence the representative points $[\phi(t), \theta(t)]$ are jointly Markovian and can be described by the transition probability density function $p[\phi(t), \theta(t)|\phi(t_o), \theta(t_o)]$ of the random variables $\phi(t) = \phi$, $\theta(t) = \theta$ at time t given the initial values $\phi(t_o) = \phi_o$ and $\theta(t_o) = \theta_o$, $t_o < t$. For brevity in notation, this distribution(density) function will be denoted by $p(\phi, \theta; t)$. This joint pdf satisfies the

2-D FP equation [37, Ch. 7, p. 329]

$$\frac{\partial p\,(\phi,\ \theta; t)}{\partial t} + \frac{\partial \mathcal{I}_{\phi}\,(\phi, \theta; t)}{\partial \phi} + \frac{\partial \mathcal{I}_{\theta}\,(\phi, \theta; t)}{\partial \theta} = 0 \tag{15}$$

with probability current densities defined by

$$\mathcal{I}_{\phi}\,(\phi, \theta; t) = \left[K_{\phi}\,(\phi, \theta) - \frac{1}{2}\left(\frac{\partial K_{\phi\phi}}{\partial \phi} + \frac{\partial K_{\phi\theta}}{\partial \phi}\right)\right] p\,(\phi,\ \theta; t) \tag{16}$$

$$\mathcal{I}_{\theta}\,(\phi, \theta; t) = \left[K_{\theta}\,(\phi, \theta) - \frac{1}{2}\left(\frac{\partial K_{\theta\theta}}{\partial \theta} + \frac{\partial K_{\theta\phi}}{\partial \theta}\right)\right] p\,(\phi,\ \theta; t)$$

and intensity coefficients given by the averages

$$K_{\phi}\,(\phi, \theta) = \lim_{\Delta t \to 0} (\Delta\phi/\Delta t)\,|\phi, \theta \tag{17}$$

$$K_{\theta}\,(\phi, \theta) = \lim_{\Delta t \to 0} (\Delta\theta/\Delta t)\,|\phi, \theta$$

with variances defined by

$$K_{\phi\phi} = \lim_{\Delta t \to 0} \left(\Delta\phi^2/\Delta t\right)|\phi, \theta; \tag{18}$$

$$K_{\theta\theta} = \lim_{\Delta t \to 0} \left[\left(\Delta\theta^2/\Delta t\right)|\phi, \theta\right]$$

and covariances defined by

$$K_{\phi\theta} = K_{\theta\phi} = \lim_{\Delta t \to 0} \left[(\Delta\phi\Delta\theta\Delta t)\,|\phi, \theta\right]. \tag{19}$$

For the composite quantum system characterized by the stochastic differential equations in (6), the intensity coefficients are readily shown to be given by

$$K_{\phi}\,(\phi, \theta) = \Delta\omega_c - (N_s\omega_c)\cos\theta\sin\phi \tag{20}$$

$$K_{\theta}\,(\phi, \theta) = \Delta\omega_c - (N_s\omega_c)\cos\phi\sin\theta$$

with variances $K = K_{\phi\phi} = K_{\theta\theta} = N_{oe}/\hbar = (\omega_c/2)\ \coth(\omega_c/2\omega_o)$ and covariances $K_{\phi\theta} = K_{\theta\phi} = 0$. Zero cross-covariances correspond to the case of isotropic fluctuations. The coefficients given in (17)–(20) serve to characterize the FP equation (15) that must satisfy the boundary condition all the time:

$$\int_{-\infty}^{\infty}\int_{-\infty}^{\infty} p\,(\phi,\ \theta; t)\,d\phi\ d\theta = 1. \tag{21}$$

Before attempting to solve this multidimensional partial differential equation it is beneficial to qualitative discuss the behavior of $p\,(\phi, \theta; t)$ with the passage of time starting from $t = t_o$. In every realization of the Markov process trajectories, the representative points (Φ, Θ) or (ϕ, θ) have a very complicated form and can be thought of as a " Brownian Particle" moving about in the (ϕ, θ) plane. When a large number of realizations are taken, these points create probability masses around the stable points (ϕ_n, θ_k) defined above; see Fig. 4. The probability density at any stable point is proportional to the probability surrounding that point.

If one starts the phase trajectories at $\phi_0 = \theta_0 = 0$ at $t = t_o$, then the quantum noise impacts are two-fold; while knocking the particle around the initial point, with the passage of time, it will be "kicked" to another stable point located in the (ϕ, θ) plane (see Figs. 4 and 6), where it remains for a short duration and the "phase kicking" process continues. The "phase-jumps" between stable points at random points in time can be regarded as a loss of quantum synchronization. The frequency of these jumps or "interruptions of quantum synchronization" are determined by the quantum signal-to-noise ratio R in (14). In the limit as t approaches infinity, the probability mass becomes uniformly spread over the entire (ϕ, θ) plane and $p\,(\phi,\ \theta; t)$ approaches zero as t approaches infinity while the variances of ϕ and θ become infinity; see Fig. 6. Since the steady state statistical behavior of the

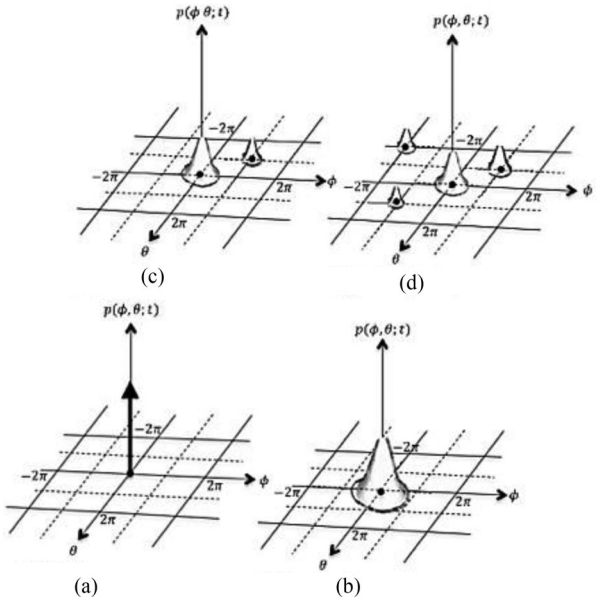

Fig. 6. Temporal evolution of $p(\phi, \theta; t)$ at $\phi_s = \theta_s = 0$.

quantum system is of utmost interest, one must look for a modified phase process which captures the pertinent statistical information of the actual processes yet yields a meaningful mathematical solution in the steady state, i.e., as $t \to \infty$. As we shall see in the next section, one way to overcome this behavior is to consider the statistical characterization of the processes $\phi(t)$ and $\theta(t)$ reduced Mod 2π.

4.1. Mod 2π Solution to the Fokker-Planck Equation

As previously mentioned, the coefficients of the FP equation are periodic in ϕ and θ. If $p(\phi, \theta; t)$ is a solution for the initial condition $p(\phi, \theta; t_0) = \delta(\phi - \phi_o)\delta(\theta - \theta_o)$ then $p(\phi + 2n\pi,\ \theta + 2k\pi; t)$ is also a solution. Define the function

$$P(\phi, \theta; t) = \sum_{n=-\infty}^{\infty} \sum_{k=-\infty}^{\infty} [p(\phi + 2n\pi,\ \theta + 2k\pi;\ t)]. \tag{22}$$

Since each term in (22) is a solution of (15), the infinite sum $P(\phi, \theta; t)$ is also a solution to (15) with $p(\phi, \theta; t)$ replaced by $P(\phi, \theta; t)$. When ϕ and θ are restricted to the probability space $|\phi| \leq \pi$ and $|\theta| \leq \pi$, $P(\phi, \theta; t)$ represents the Mod 2π solution to the FP equation. Notice that (22) sums the probability mass "build-ups" around the set of stable points (ϕ_n, θ_k), as illustrated in Figs. 4 and 6. In essence they have been overlaid on a square of side length 2π centered at the origin. The Mod 2π phase-space $S(\phi, \theta) = [(\phi, \theta);\ |\phi| \leq \pi,\ |\theta| \leq \pi]$ can also be viewed as a square flat torus which can be rolled up into a Clifford horn torus. This implies that the Mod 2π distribution $P(\phi, \theta; t)$ lives on the torus $T^2 = S^1 \times S^1 \epsilon\, \mathbb{R}^3$.

Since the probability mass $p(\phi, \theta; t)$ must be conserved as in (21), one requires that

$$\int_{-\pi}^{\pi} \int_{-\pi}^{\pi} P(\phi, \theta; t)\, d\phi d\theta = 1. \tag{23}$$

Moreover, the "folding or wrapping process" alleviates the infinite variance issues associated with $p(\phi, \theta; t)$ in the steady state. However, to give a complete statistical description of the joint process $[\phi(t), \theta(t)]$ introduces the need to specify the average rates of "phase-jumping" between the stable points, (ϕ_n, θ_k), viz., the polarization phase flips and phase slip rates, say S_π *and* $S_{2\pi}$. Polarization slips of 2π multiples occur when the quantum system state moves from the vicinity of

the stable points ($\phi_n = 2\pi n,\ \theta_k = 2\pi k$) to ($\phi_m = 2\pi m,\ \theta_l = 2\pi l$) for all $n,\ k,\ m, l$ and $(n, k) \neq (m, l)$ while polarization flips occur when the quantum system state moves from the vicinity of the state ($\phi_n = 2\pi n,\ \theta_k = 2\pi k$) to the vicinity of the stable points ($\phi_m = (2\pi m + 1)\pi,\ \theta_l = (2\pi l + 1)\pi$); see Figs. 4 and 6. These random movements represent interruptions in the state of quantum polarization of the quantum system. Of course, for large values of the quantum system energy-to-noise ratio R, such phase-jumps are expected to be infrequent while for low values of R, losses in quantum synchronization are expected to be more frequent [34], [37]. At very low values of R, all polarization states become equiprobable.

4.2. Steady State Modulo 2π Solution to the Fokker-Planck Equation

Unfortunately, investigation of "transient processes" by solving the non-stationary FP equation (15) with $p(\phi,\ \theta; t)$ replaced by $P(\phi,\ \theta; t)$ is a difficult problem. In this regard, the method of separation of variables can be used to turn the problem into a two point boundary problem in search of a set of eigenvalues and a set of orthogonal functions. On the other hand, a case of great interest is the stationary coherency distribution $P(\phi,\ \theta)$ corresponding to the following condition:

$$\lim_{t\to\infty} \frac{\partial P(\phi,\ \theta; t)}{\partial t} = 0 \tag{24}$$

assuming the steady state solution $P(\phi,\ \theta)$ exists. Using this condition in (15), the stationary distribution $P(\phi,\ \theta)$ satisfies the steady state FP equation

$$\frac{\partial \mathcal{I}_\phi(\phi,\theta)}{\partial\phi} + \frac{\partial \mathcal{I}_\theta(\phi,\theta)}{\partial\theta} = 0 \tag{25}$$

with time-independent probability currents

$$\begin{aligned} \mathcal{I}_\phi(\phi,\theta) &= K_\phi(\phi,\theta)\, P(\phi,\theta) - (K/2)\,\partial P(\phi,\theta)/\partial\phi \\ \mathcal{I}_\theta(\phi,\theta) &= K_\theta(\phi,\theta)\, P(\phi,\theta) - (K/2)\,\partial P(\phi,\theta)/\partial\theta \end{aligned} \tag{26}$$

where $K = N_{oe}/\hbar = (\omega_c/2)\ \coth(\omega_c/2\omega_o)$ and $K_\phi(\phi,\theta)$ and $K_\theta(\phi,\theta)$ given by (20). Furthermore, from (20) it is noted that

$$\frac{\partial K_\phi(\phi,\theta)}{\partial\theta} = \frac{\partial K_\theta(\phi,\theta)}{\partial\phi} = (\omega_c N_s)\sin\phi\ \sin\theta \tag{27}$$

which establishes the potential condition for isotropic fluctuations [37]. Thus, the probability currents in (16) vanish on the boundaries of the probability space thereby suggesting that $P(\phi,\theta)$ is reminiscent of a Boltzman like distribution for which $P(\phi,\theta) = \exp[U(\phi,\theta)]$ where the potential function $U(\phi,\theta)$ is defined by the total differential

$$dU(\phi,\theta) = \frac{\partial U(\phi,\theta)}{\partial\phi}d\phi + \frac{\partial U(\phi,\theta)}{\partial\theta}d\theta. \tag{28}$$

For isotropic fluctuations, one can use the boundary conditions and the solution $P(\phi,\theta) = \exp[U(\phi,\theta)]$ in (25) and (26) to show that

$$\frac{\partial U}{\partial\phi} = 2K_\phi(\phi,\theta)/K;\ \ \frac{\partial U}{\partial\theta} = 2K_\theta(\phi,\theta)/K. \tag{29}$$

Upon substitution of (29) into (28), one can write the potential function in (28) as the line integral

$$U(\phi,\theta) = (2/K)\int\left[K_\phi(\phi,\theta)\,d\phi + K_\theta(\phi,\theta)\,d\theta\right] - \ln N \tag{30}$$

where N is the constant of integration determined by the normalization condition. Substitution of (20) into (30) leads to the potential function

$$U(\phi,\theta) = (\Delta F/F)(\phi+\theta) + 2R\cos\phi\cos\theta - \ln N \tag{31}$$

where R is defined in (14), and

$$\left(\frac{\Delta F}{F}\right) = \left(\frac{4\Delta\nu_c}{\nu_c}\right)\tanh\left(\frac{\nu_c}{2\nu_o}\right) \tag{32}$$

represents the frequency decoherence parameter. Thus the coherence distribution is given by

$$P(\phi,\theta) = exp\left[(\Delta F/F)(\phi+\theta) + 2Rcos\phi cos\theta\right]/N. \tag{33}$$

When $\Delta F/F \neq 0$ in (33), one can relate the frequency decoherence parameter to fiber optic cable birefringence $\beta(\omega)$ and the communication bandwith $W\ Hz$. Since $\beta(\omega) = (\Delta n/c)\omega$ [39], it is each to show that the dispersion bandwidth $\Delta\nu_c \cong \delta W$ is related to the channel birefringence (PMD) as $\Delta\beta = (\Delta n/c)[\beta(\omega) - \beta(\omega_c)] = (\Delta n/c)/\delta W$; $0 \leq \delta \leq 1$. When ϕ and θ are small ($R \gg 1$), $\cos x \cong 1 - x^2/2$ and $P(\phi,\theta)$ in (33) is approximated the bivariate Gaussian distribution for independent random variables with equal means $R(\Delta F/F)$ and variances $\sigma_\phi^2 = \sigma_\theta^2 \approx 1/2R$. Thus the presence of frequency decoherence produces a bias in the prepared Q-SoP (ϕ_s, θ_s). Using integral formulas and results given in the Appendix and with (33) substituted into (23), one can show that

$$N = 2\pi\sum_{k=0}^{\infty}\epsilon_k C_k\left|I_{(k/2+i\Delta F/F)}(R)\right|^2 \tag{34}$$

where $I_v(x)$ is the imaginary Bessel function of imaginary order, and

$$C_k = 2\pi\exp(\Delta F/F)\left[\sinh(\pi(\Delta F)/F)/((\Delta F)/F)\right]/\left[(\Delta F/F)^2 + k^2\right] \tag{35}$$

for $k = 1,\ 2, \ldots and$ for $k = 0$,

$$C_0 = 2\pi\exp\left(\frac{2\Delta F}{F}\right)\sinh\left(\frac{\pi\Delta F}{F}\right)/(\pi\Delta F/F). \tag{36}$$

When $\triangle F/F = 0$, then $C_k = 0$ for all $k \neq 0$, $C_0 = 2\pi$, $N = 4\pi^2 I_0^2(R)$, and the coherency distribution reduces to

$$P(\phi,\theta) = \exp\left[2Rcos\phi cos\theta\right]/\left[2\pi I_0(R)\right]^2 \tag{37}$$

for $|\phi| = |\theta| \leq \pi$. The Mod 2π process in ϕ and θ characterized by (37) can be mapped onto the unit Majorana sphere by reducing the ϕ(t) trajectories Mod 2π and the θ(t) trajectories Mod π. When this is done, the coherence distribution $P_\pi(\phi,\theta)$ for this process is related to the Mod 2π process characterized by (37) as $P_\pi(\phi,\theta) = 2\ P(\phi,\theta)$ for $\phi \leq \pi$, $0\ \leq \theta \leq \pi$.

Figs. 7 and 8 illustrate this probability distribution on the unit sphere; it is clear that the distribution is non-Gaussian and multimodal. Fig. 7 shows transparency distributions for various values of R while Fig. 8 demonstrates this distribution as seen from the North and South Poles (NP and SP) view.

Fig. 9 demonstrates transparency distributions for the three regions of system operation suggested in Fig. 5, viz., the high temperature (or low frequency) Regions I and II and the low temperature (or high frequency) Region III. Notice how the probability masses transition from highly diffuse over the sphere to more concentrated as one transitions from low values of R to higher values. From these figures one observes probability mass buildups around the stable points represented as NP and SP. These probability mass buildups demonstrates the statistical dynamics that coherent polarized states undergo in the presence of quantum noise.

The "phase-jumping" process that takes place between stable polarization points (North-South Poles) can best be discussed from the Cartesian phase-space perspective. For this reason, the Mod 2π coherency distribution $P(\phi,\theta)$ has been plotted in Cartesian coordinates in Fig. 10 for R $= 2$. The decoherence affects manifest themselves in the form of qubit flips and slips caused by quantum noise impacts upon the coherent polarized states characterized in (3). It is evident that this distribution is also non-Gaussian and multi-modal.

The probability mass located on the square flat torus $|\phi| \leq \pi$, $|\theta| \leq \pi$ of Fig. 10 can be folded to render a Clifford horn torus. When the coherency distribution in Fig. 10 is viewed from the

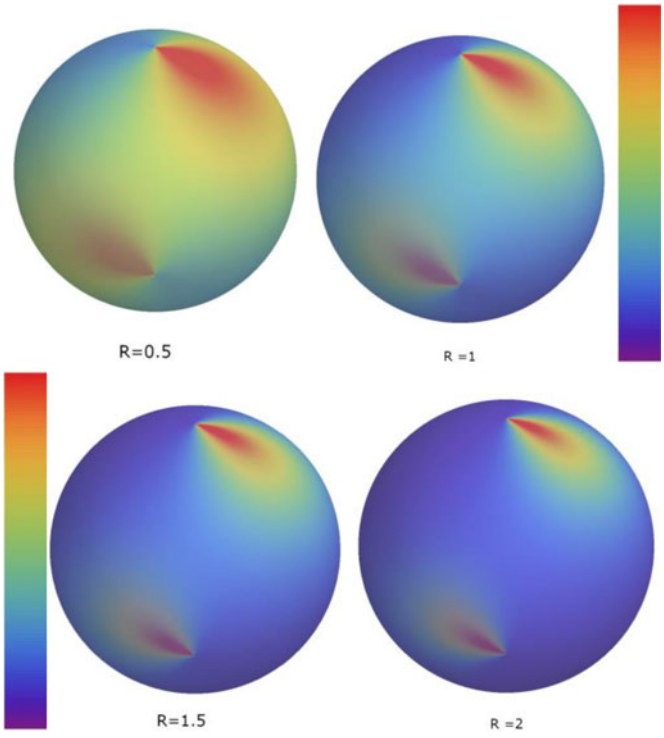

Fig. 7. Transparent coherency distribution $P_\pi(\phi, \theta)$ for various values of R.

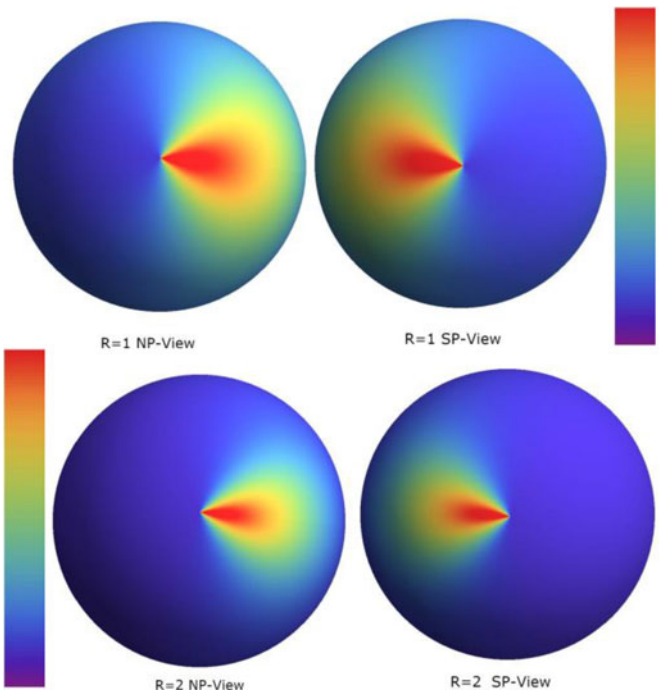

Fig. 8. North and South Poles (NP and SP) view of coherency distribution $P_\pi(\phi, \theta)$ for various values of R.

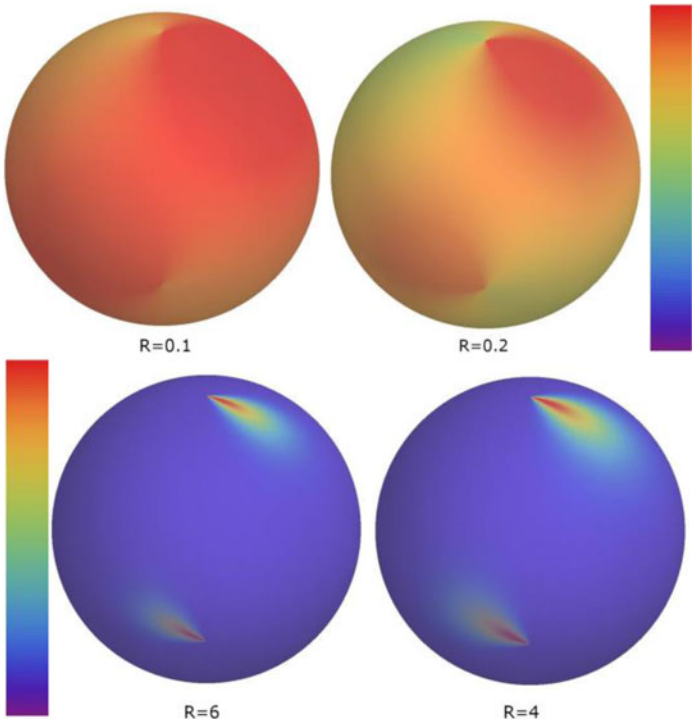

Fig. 9. Transparency distribution $P_{\pi}(\phi, \theta)$ for the regions of system operation shown in Fig. 4.

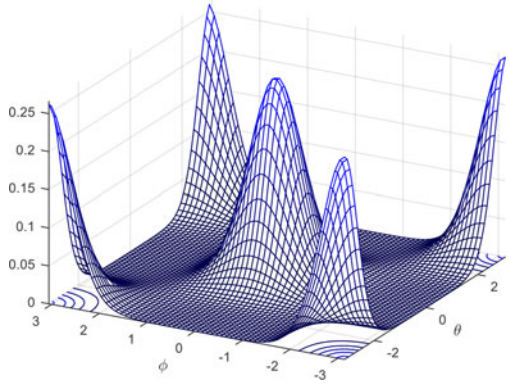

Fig. 10. Coherency distribution $P(\phi, \theta)$ for R = 2.

perspective of living on the Clifford horn torus, the four corner points (π, π), $(-\pi, -\pi)$, $(-\pi, \pi)$ and $(\pi, -\pi)$ located on the square flat torus map to the same point on the Clifford torus which is antipodal with respect to the point (0,0). Assuming the original polarization state is prepared for $\phi_s = \theta_s = 0$, then when the QS looses synchronization and flips to the antipodal state, it has re-established itself in a "phase-flip" condition. To overcome this condition some form of mitigation will have to be used, e.g., a quantum error correcting code, etc. [23], [24], [38], [40].

Finally, the potential function $U(\phi, \theta) = 2R cos\theta cos\phi$ in (37) is plotted in Fig. 11 below for $\Delta F/F = 0$; here the "peaks" in the "egg-like" carton represent potential maximum in the coherency distribution and the egg carton bottoms are potential minimums, i.e., places of minimum probability.

Furthermore, since $\phi = \Phi - \phi_s$ and $\theta = \Theta - \theta_s$, the conditional distribution of the Q-SoP (Φ, Θ) is given by

$$P(\Phi, \Theta|\phi_s, \theta_s) = \exp[2R\cos(\Phi - \phi_s)\cos(\Theta - \theta_s)]/4\pi^2 I_0^2(R) \quad (38)$$

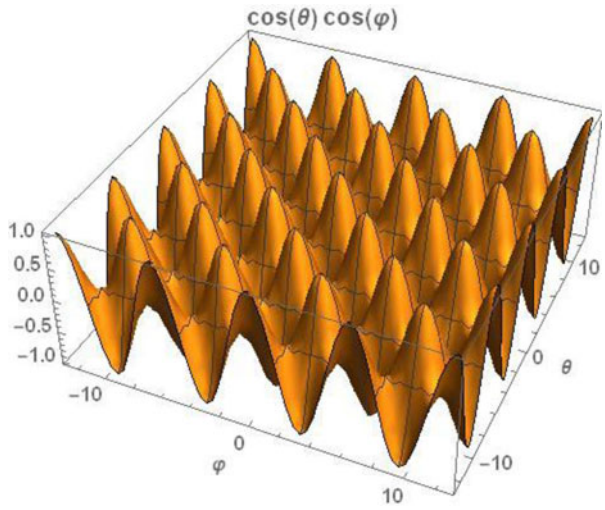

Fig. 11. Normalized potential function $U(\phi, \theta)/2R$ versus (ϕ, θ).

for $|\Phi - \phi_s| \leq \pi$, $|\Theta - \theta_s| \leq \pi$.

When quantum noise is dominate in the composite quantum system, then $R \ll 1$ and the coherency distribution in (37) becomes

$$\lim_{R \to 0} P(\phi, \theta) = 1/4\pi^2 \tag{39}$$

which is the uniform distribution over the phase-space. For the case where the polarization state dominates (high energy-to-noise ration $R \gg 1$) one expects small quantum noise fluctuations about the polarized signal state (ϕ_s, θ_s). Thus, one can use the approximation $I_o(x) \approx \exp(-x)/\sqrt{2\pi x}$ and $\cos y \approx 1 - y^2/2$ in (38) and show that

$$\lim_{R \to \infty} P(\Phi, \Theta | \phi_s, \theta_s) \to \lim_{R \to \infty} \frac{\exp\left\{\left[-(\Phi - \phi_s)^2 - (\Theta - \theta_s)^2\right]/2(2R)^{-1}\right\}}{2\pi(2R)^{-1}} = \delta(\Phi - \phi_s)\,\delta(\Theta - \theta_s) \tag{40}$$

which implies that the noise fluctuations ϕ and θ become uncorrelated, zero-mean identically distributed random variables with equal variances, $(2R)^{-1}$. However, linearization of the equations of operation in (5) alleviate the notions of polarizations phase-flips and phase-slips.

5. Quantum Degree-of-Polarization (Q-DoP) and Other Marginal Distributions

As shown in the previous sections, quantum polarization states can loose their orientation in a decoherence process attributed to a noisy environment. A measure of decoherence is the qubit orientation, i.e., direction of electric field characterized statistically by the Q-DoP distribution. If one defines the Q-DoP as the z-component, say $P_z = \cos\theta$, then the joint coherency distribution in (37) becomes the joint distribution

$$P(\phi, P_z) = \exp(2RP_z \cos\phi)/2\pi^2 I_o^2(R)\sqrt{1 - P_z^2} \tag{41}$$

for $|\phi| \leq \pi$ and $|P_z| \leq 1$. From the three joint distributions (37), (38), and (41), various marginal and conditional probability distributions are forthcoming and are useful in accessing the longitudinal and azimuthal phase jitters. The marginal probability distributions $P(\phi)$ and $P(\theta)$ are of interest in accessing the quantum jitter performances. Using the fact that

$$I_o(x) = \int_{-\pi}^{\pi} \exp(x\cos\phi)d\phi/2\pi = \int_0^{\pi} \exp(x\cos\phi)d\phi/\pi \tag{42}$$

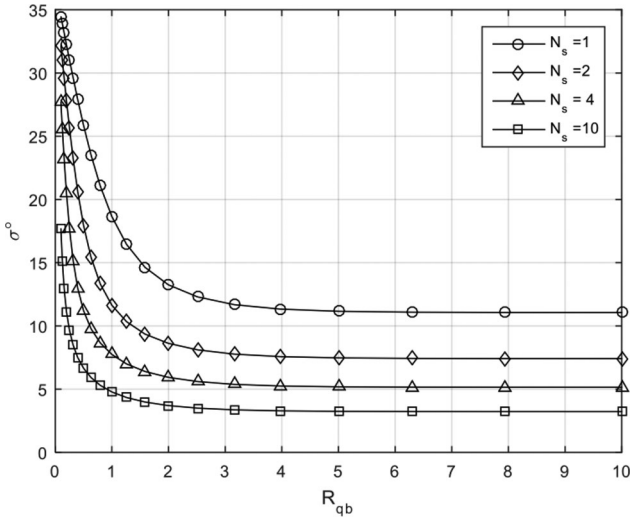

Fig. 12. Polarization jitter in degrees versus R_{qb} with the number of photons a parameter.

the marginal distributions for ϕ and θ become

$$P(\phi) = \int_{-\pi}^{\pi} P(\phi,\ \theta)\, d\theta = I_o(2R\cos\phi)/2\pi I_o^2(R) \tag{43}$$

$$P(\theta) = \int_{-\pi}^{\pi} P(\phi,\ \theta)\, d\phi = I_o(2R\cos\theta)/2\pi I_o^2(R)$$

for $|\phi| \leq \pi$, $|\theta| \leq \pi$. Furthermore, using (41) and (42), the Q-DoP distribution becomes

$$P(P_z) = \int_{-\pi}^{\pi} P(\phi,\ P_z)\, d\phi = \frac{I_o(2RP_z)}{\pi I_o^2(R)\sqrt{1-P_z^2}} \tag{44}$$

for $|P_z| \leq 1$. Finally, the conditional distributions $P(\phi|\theta)$, $P(\theta|\phi)$, $P(Q_z|\phi)$ and $P(\phi|P_z)$ can be readily derived from (37) and (41) using Bayes rule. These are given by

$$P(\phi|\theta) = \exp[2R\cos\phi\cos\theta]/2\pi I_o(2R\cos\theta) \tag{45}$$

$$P(\theta|\phi) = \exp[2R\cos\phi\cos\theta]/2\pi I_o(2R\cos\phi)$$

and

$$P(\phi|P_z) = \exp\left[2RP_z\cos\phi\right]/2\pi I_o\left(2RP_z\right) \tag{46}$$

$$P(P_z|\theta) = \exp\ \left[2RP_z\cos\theta\right]/\pi\ I_o(2R\cos\theta)\ \sqrt{1-P_z^2}\Big).$$

Such distributions are useful in assessing the performance of quantum communication systems disturbed by quantum noise, [10]. Fourier series can be obtained for these distributions using results in the Appendix.

6. Sum and Difference Distributions, Circular Moments and Frequency Decoherence Moments

Define the sum θ_+ and the difference θ_- random variables $\theta_\pm = \phi \pm \theta$. Then using (37) and the cosine product identity, the *Mod* 2π joint distribution of these random variables transforms to

$$P(\theta_+, \theta_-) = \exp[R(\cos\theta_+ + \cos\theta_-)]/4\pi^2 I_o^2(R) = P(\theta_+)\, P(\theta_-) \tag{47}$$

for $|\theta_+| \leq \pi,\ |\theta_-| \leq \pi$. Thus, θ_+ and θ_- are Stratonovich-Tikhonov-Viterbi distributed [37, Ch. 9].

The circular moments $\cos n\phi$, $\sin n\phi$ and $\cos n\theta$, $\sin n\theta$ are of interest in assessing "frequency-decoherence" averages $\dot{\phi}$ and $\dot{\theta}$ from (6). For $\Delta\nu_c = 0$, these are readily found by expanding the coherence distribution into a double Fourier series using the Jacob-Anger formula see (A-0 in the Appendix)

$$\exp(z\cos x) = \sum_{k=0}^{\infty} \epsilon_k I_k(z)\cos nx \tag{48}$$

where $\epsilon_k = 1$ for $k = 0$ and $k = 2$ for all $k > 0$ and the integral formula

$$\int_0^{\frac{\pi}{2}} \cos(2\mu x)\, I_{2\nu}(2a\cos x)dx = (\pi/2)\, I_{\nu-\mu}(a)\ I_{\nu+\mu}(a). \tag{49}$$

In particular, the circular moments are readily found from

$$\sin(n\phi) = \int_{-\pi}^{\pi} \sin(n\theta)\, P(\theta)\, d\theta;\ \cos(n\phi) = \int_{-\pi}^{\pi} \cos(n\phi)\, P(\phi)\, d\phi \tag{50}$$
$$\sin(n\theta) = \int_{-\pi}^{\pi} \sin(n\phi)\, P(\phi)\, d\phi;\ \cos(n\theta) = \int_{-\pi}^{\pi} \cos(n\theta)\, P(\theta)\, d\theta$$

using (43), (49), and the Fourier Series for $I_o[\text{acos}(x)]$ of the Appendix. Substitution of (43) into (50) and using (49), it follows that $\sin(n\phi) = \sin(n\theta) = 0$ while

$$\cos(n\phi) = \cos(n\theta) = I_{-n/2}(R)\, I_{n/2}(R)/I_o^2(R) \tag{51}$$

for $= 0, 1, 2, \ldots$. Finally, from (6) the mean value of the frequency decoherence effects are given by

$$<\dot{\phi}>= 2\pi[\Delta\nu_c - N_s\nu_c <\cos\theta\sin\phi>] \tag{52}$$
$$<\dot{\theta}>= 2\pi[\Delta\nu_c - N_s\nu_c <\cos\phi\sin\theta>].$$

When the frequency decoherence variable $\Delta\nu_c = 0$, then $<\dot{\phi}>=<\dot{\theta}>= 0$. When $\Delta\nu_c \neq 0$, the frequency decoherence moments can be determined using (33).

7. Polarization State Jitter

Since the Mod 2π reduced coherency distribution is bimodal, a quantum error correcting code [23]–[25] will be required to eliminate errors due to polarization flips. In this regard, the polarization state jitter associated with each stable point is of practical interest. Recall from Fig. 3 and Section II-A that the $Mod\ 2\pi$ phase plane separatrix solution curves partitioned the probability space into two disjoint regions. These saddle point separatrix separated the phase plane into regions in which all solution curves tend to one of two stable singularities, i.e., one which probability flows to the origin, say the right handed circular polarization state, and the other state which is antipodal, say left handed circular polarization. When quantum error correcting coding is used the polarization state jitter with respect to each stable singularity is of interest. Considering the origin to be the state that is "inside" the separatrix solution curves and the antipodal state corresponds to the "outside" solution curves, one can write the polarization jitter variance with respect to ϕ and θ relative to the origin as

$$\sigma^2 = {\sigma_\theta}^2 = \sigma_\phi^2 = 4\int_0^{\pi} \phi^2 d\phi \int_0^{\pi-\phi} P(\phi,\theta)\, d\theta \tag{53}$$

where solution symmetry has been used. To no avail, integration in (53) can be performed using the double Fourier series expansion given in the Appendix for $P(\phi, \theta)$; thus, numerical integration is preferred. Plotted in Fig. 12 are the standard deviations $\sigma_\phi = \sigma_\theta = \sigma$ for various values of the system parameters N_s and R_{qb}. From this figure one notes the importance use of energy scaleability to

reduce polarization jitter. One may also conclude that single-photon communications using quantum polarization modulation and a quantum error correcting code is possible, however, reliable quantum communication using "coherent polarized state" packets containing three to four photons is definitely achievable.

8. Conclusion

A dynamical model for the polarization state of a coherent quantum system embedded in a thermal radiation environment has been proposed. This model is characterized by coupled stochastic differential equations mimicking mutually-coupled pendulums driven by quantum phase noise. By taking advantage of the Markovian nature of the noise, a Fokker-Planck equation is specified whose solution yields a quantum system coherency distribution from which other useful probability distributions that characterize quantum decoherence effects are derived. At the heart of the stability of a coherent quantum system is a quantum synchronization phenomenon that breaks down at an average rate which depends upon the quantum system energy-to-noise ratio, i.e., polarization interruptions occur and lead to quantum system polarization flips and slips. From the coherency distribution and its by-products, quantum polarization phase jitter variances leading to decoherence in quantum superposition states are derived and plotted. The results presented will find applications to the problem of evaluating single and multiphoton communication system performance and in the system engineering design of quantum communication systems and a quantum internet connecting quantum computers.

Appendix
Expansion of $P(\phi, \theta)$ into a Doubly Infinite Fourier Series

Assume that $\Delta\nu_c = 0$. Using the Jacob Anger formula

$$\exp\ (zcosx) = \sum_{k=0}^{\infty} \epsilon_k I_k\,(z)\,coskx$$

one can expand the coherency distribution into a Fourier series

$$P\,(\phi, \theta) = \left[4\pi^2 I_0^2\,(R)\right]^{-1} \sum_{k=0}^{\infty} \epsilon_k I_k\,(2R\cos\theta)\cos\,(k\phi) \tag{A-1}$$

where $\epsilon_k = 1$ for $k = 0$ and $k = 2$ for $k \geq 1$. Upon using the integral formula

$$\int_0^{\frac{\pi}{2}} \cos\,(2\eta x)\, I_{2\nu}\,(2\mathrm{R}\cos x)\, dx = (\pi/2)\, I_{\nu-\eta}\,(R)\, I_{\nu+\eta}\,(R) \tag{A-2}$$

$I_k(2R\cos\theta)$ can be expanded into the Fourier series

$$I_k\,(2R\cos\theta) = \sum_{l=0}^{\infty} a_{kl}\cos l\theta \tag{A-3}$$

where, from (A-2)

$$a_{kl} = \frac{2}{\pi}\int_0^{\frac{\pi}{2}} \cos\,(l\theta)\, I_k\,(2R\cos\theta)\, d\theta = I_{\frac{k-l}{2}}\,(R)\, I_{\frac{k+l}{2}}\,(R)\ \ I_k\,(2Rcos\theta) = \sum_{l=0}^{\infty} I_{\frac{k-l}{2}}\ \ (R)\, I_{\frac{k+l}{2}}\ \ (R)\cos\,(l\theta)\,. \tag{A-4}$$

Substitution of (A-4) into (A-1) leads to the doubly infinite Fourier series

$$P\,(\phi, \theta) = \sum_{k=0}^{\infty}\sum_{l=0}^{\infty} \epsilon_k I_{\frac{k-l}{2}}\ \ (R)\, I_{\frac{k+l}{2}}\ \ (R)\cos l\theta coskl\phi/4\pi^2 I_0^2\,(R)\,. \tag{A-5}$$

The marginal $P(\phi)$ and $P(\theta)$ in (43) are readily found using this series A-1. In addition, the polarization jitters given in (52) and (53) are readily determined from $P(\phi)$ and $P(\theta)$ given in (43). For $\Delta v_c \neq 0$, repeated use of the above formulas and the result

$$\int_0^{\pi/2} \cosh(2D_1 y)\, I_o(2D_2 \cos y)\, dy = \left(\frac{\pi}{2}\right) I_{iD_1}(D_2)\, I_{-iD_1}(D_2) \tag{A-6}$$

provides N in (33) and (34). The algebraic details are omitted here for brevity of presentation.

Acknowledgment

The author would like to thank G. Velu and S. M. Aboutorabi for their typing of the manuscript and for drawing the figures not requiring numerical computations, as well as R. Grados for the numberical work as it relates to figures and for his many discussions.

References

[1] M. Legre, M. Wegmuller, and N. Gisin, "Quantum phase measurement of the degree of polarization of a light beam," *Phys. Rev. Lett.*, vol. 91, 2003, Art. no. 167902.
[2] A. B. Klimov, W. L. Sancheg-Soto, E. C. Yustas, J. Soderman, and G. Bjork, "Distance-based degree & polarization for a quantum field," *Phys. Rev. A*, vol. 72, 2005, Art. no. 033813.
[3] J. C. do Nascimento and R. V. Ramos, "Dynamics of the polarization in a depolarizing channel," *Microw. Opt. Technol. Lett.*, vol. 47, no. 5, pp. 497–500, Dec. 2007.
[4] A. Mecozzi, C. Antonelli, and M. Brodsky, "Statistics of the polarization mode dispersion dynamics," *Opt. Lett.*, vol. 32, no. 20, pp. 3032–3034, 2007.
[5] W. H. Zurek, "Decoherence, einselection, and the quantum origins of the classical," *Rev. Mod. Phys.*, vol. 75, 2003, Art. no. 715.
[6] W. H. Zurek, "Decoherence and the transition from quantum classical-Revisited," *Los Alamos Sci.*, vol. 27, pp. 2–25, 2002.
[7] A. B. Klimov, J. L. Romero, and L. L. Sanchez-Soto, "Simple quantum model for light depolarization," *J. Opt. Soc. Amer. B*, vol. 23, no. 1, pp. 126–133, Jan. 2006.
[8] A. B. Klimov, J. L. Romero, L. L. Sanchez-Soto, A. Messina, and A. Napoli, "Quantum light polarization: The phase-space perspective," *Phys. Rev. A*, vol. 77, 2008, Art. no. 033853.
[9] R. J. Glauber, "Coherent and incoherent states of radiation field," *Phys. Rev.*, vol. 131, no. 6, Sep. 1963, Art. no. 2766.
[10] W. C. Lindsey and R. Grados, "Binary quantum communication system performance in the presence of quantum noise," *IEEE Trans. Quantum Electron.*, to be published, Also see EE Dept., Univ. Southern Calif., TR-061517, Los Angeles, CA, USA.
[11] A. R. Usha, A. K. Rajagopal, Shuda, H. S. Karthik, and J Prabhu Tej, "Non-classicality and entanglement of symmetric multiqubit states," to be published.
[12] C. W. Gardiner and P. Zollar, *Quantum Noise*. Berlin, Germany: Springer-Verlag, 2004.
[13] C. Huygens, *Oeuvres Complêtes de Christiaan Huygens*. vol. 17, p. 183, Martinus Nijhoff, The Hague, The Netherlands, 1932.
[14] W. C. Lindsey and J. M. N. Periera, *Christian Huygens: Mutual Space-Time Synchronization Between Clocks*. Amherst, MA, USA: Dibner Library, Univ. Mass., 1991.
[15] E. Majorana, "Atomi orientati in campo magnetico variabile," *Nuovo Cimento*, vol. 9, pp. 43–50, 1932.
[16] G. Bjork, A. B. Klimov, P. de la Hoz, M. Grassl, G. Leuchs, and L. L. Sanchez-Soto, "Extremal quantum states and their majorana constellations," *Phys. Rev. A*, vol. 92, 2015, Art. no. 031801(R).
[17] H. Makela and A. Messina, "N-qubit states as points on the bloch sphere," *Phys. Soc.*, vol. T140, 2010, Art. no. 014054.
[18] P. Ribeiro and R. Mosseri, "Entanglement in the symmetric sector of n-qubits," *Phys. Rev. Lett.*, vol. 106, no. 18, May 2011, Art. no. 180501.
[19] M. Aulbach, "Symmetric entanglement classes for n-qubits," *Phys. Rev. Lett.*, vol. 103, Jan. 2011, Art. no. 070503.
[20] J. Martin, D. Giraud, P. A. Braun, D. Braun, and T. Bastin, "Multiqubit states with high geometric entanglement," *Phys. Rev. A*, vol. 81, 2010, Art. no. 062347.
[21] M. Aulbach, D. Markham, and M. Murao, "Geometric entanglement of symmetric states and the majorana representation," *Proc. SPIE*, vol. 6519, pp. 141–158, 2011.
[22] J. Zimba, "Anticoherent spin states via the majorana representation," *Electron. J. Theoretical Phys.*, vol. 3, no. 10, pp. 143–156, 2006.
[23] P. W. Shor, "Scheme for reducing decoherence in quantum computer memory," *Phys. Rev. A*, vol. 52, 1995, Art. no. R2493.
[24] A. M. Steane, "Efficient fault-tolerant quantum computing" *Nature*, vol. 399, pp. 124–126, 1999.
[25] M. M. Wilde, *Quantum Information Theory*. Cambridge, U.K.: Cambridge Univ. Press, 2013.
[26] C. W. Helstrom, *Quantum Decision and Estimation Theory*. New York, NY, USA: Academic, 1976.
[27] J. I. Cirac, P. Zoller, H. J. Kimble, and H. Mabuchi, "Quantum state transfer and entanglement distribution among distant nodes in a quantum network," *Phys. Rev. Lett.*, vol. 78, 1997, Art. no. 3221.

[28] C. H. Bennett and G. Brassard, "Quantum cryptography: Public key distribution and coin tossing," *Proc. Int. Conf. Comput., Syst. Signal Process.*, 1984, pp. 175–179.
[29] W. C. Lindsey, M. K. Simon, and S. M. Hinedi, *Digital Communications*. Englewood Cliff, NJ, USA: Prentice-Hall, 1995.
[30] E. Alfser and F. Shultz, "Unique decompositions, focus and automorphisms of separable states," *J. Math. Phys.*, vol. 51, 2010, Art. no. 052201.
[31] M. A. Nielsen and J. Kempe, "Separable states are more disordered globally than locally," *Phys. Rev. Lett.*, vol. 86, no. 22, pp. 5184–5187, May 2001.
[32] T. Bastin, S. Krins, P. Mathonet, M. Godefroid, L. Lamata, and E. Salano, "Operational families of entanglement classes for symmetric N-Qubit states," *Phys. Rev. Lett.*, vol. 103, 2009, Art. no. 070503.
[33] A. Strelstov, U. Singh, H. S. Dhar, M. N. Bera, and G. Adesso, "Measuring quantum coherence with entanglement," *Phys. Rev. Lett.*, vol. 115, Jun. 2015, Art. no. 020403.
[34] M. Xu, D. A. Tieri, E. C. Fine, J. K. Thompson, and M. J. Holland, "Quantum synchronization of two ensembles of atoms," *Phys. Rev. Lett.*, vol. 113, Oct. 2014, Art. no. 154101.
[35] M. D. Eisaman, J. Fan, A. Migdall, and S. V. Polyakov, "Single photon sources and detectors," *Rev. Scientific Instrum.*, vol. 82, 2011, Art. no. 07110, doi: 10.106311.3610677
[36] H. T. Davis, *Introduction to Nonlinear Differential and Integral Equations*. Washington, DC, USA: U.S. Atomic Energy Commission, 1961.
[37] W. C. Lindsey, *Synchronization Systems in Communication and Control*. Englewood Cliffs, NJ, USA: Prentice-Hall, 1972.
[38] M. Sucamarini, G. D. Giuseppe, S. Damodarakurup, Dr. Vitali, and P. Tombesi, "Suppression of polarization decoherence for traveling light pulse via Bang-Bang dynamical decoupling," *Phys. Rev. A*, vol. 83, Jan. 2011, Art. no. 032320.
[39] V. I. Kaminov, T. Li, and A. E. Willner, "*Optical Fiber Telecommunications*. New York, NY, USA: Academic, 2008, ch. 17.
[40] J. Chiaverini *et al.*, "Realization of quantum error correction," *Nature*, vol. 432, pp. 602–605, 2004.